

Multivariable Feedback Combustion Control

The development of a control system using an in-cylinder pressure sensor

Master's thesis in Electrical Engineering

AMANDA LARSSON
GABRIELLA LYGNSTRAND

MASTER'S THESIS EX055/2018

Multivariable Feedback Combustion Control

The development of a control system using an
in-cylinder pressure sensor

AMANDA LARSSON
GABRIELLA LYGNESTRAND



CHALMERS
UNIVERSITY OF TECHNOLOGY

Department of Electrical Engineering
Division of Systems and Control
Automatic Control
CHALMERS UNIVERSITY OF TECHNOLOGY
Gothenburg, Sweden 2018

Multivariable Feedback Combustion Control
The development of a control system using an
in-cylinder pressure sensor
AMANDA LARSSON
GABRIELLA LYGNESTRAND

© AMANDA LARSSON & GABRIELLA LYGNESTRAND, 2018.

Supervisor: Johan Engbom, Volvo Group Truck Technology
Examiner: Torsten Wik, Department of Electrical Engineering

Master's Thesis EX055/2018
Department of Electrical Engineering
Division of Systems and Control
Automatic Control
Chalmers University of Technology
SE-412 96 Gothenburg
Telephone +46 31 772 1000

Cover: In-cylinder pressure curve.

Typeset in L^AT_EX
Gothenburg, Sweden 2018

Multivariable Feedback Combustion Control
The development of a control system using an
in-cylinder pressure sensor
AMANDA LARSSON & GABRIELLA LYGNESTRAND
Department of Electrical Engineering
Chalmers University of Technology

Abstract

The development of a linear quadratic controller to manipulate diesel injections in an engine is presented in this thesis. An in-cylinder pressure sensor is used to estimate the two states used in the controller; torque and crank angle degree when 50 % of the fuel has burnt off. Also, two different methods for detection of a pilot injection have been investigated.

The estimation of crank angle degree when 50 % of the fuel has burned off was determined using Heywood's formula for heat release calculations. Reasonable results were obtained in both simulations and engine tests. The first method for the pilot detection is a form of pattern recognition using convolution with the derivative of the heat release rate. The second method for the pilot detection compares the pressure with a reference curve without injections. Both methods worked in simulations, but only the second method gave valid results in engine tests.

The controller performed well for the torque, but has a steady state error for crank angle degree when 50 % of the fuel has burnt off, when the introduced error is large. The developed controller can contribute to correcting errors from e.g. worn engine parts and differences in fuel qualities.

Keywords: In-cylinder pressure sensor, Torque, CA50, Pilot detection, Multivariable control, Linear quadratic controller

Acknowledgements

Without the help from numerous people, this project would not have been possible. First, we would like to send our greatest appreciation to our supervisor at Volvo Group Trucks Technology (GTT) Johan Engbom, for supporting us in our work with his knowledge and devotion. We also would like to thank our examiner at Chalmers, Professor Torsten Wik, who has contributed with support and good discussions during the project. A big thank you also goes to Anton Kjellin who has helped us in numerous ways, for instance with good discussions and technical support. Many others have helped us during the project and also deserves our deepest gratitude; Igor Lumpus, Mikael Svensson, and Fabian Hasselby from GTT, and also Gabriel Turesson from Lund University, among others.

Amanda Larsson & Gabriella Lygnerstrand, Gothenburg, June 2018

Contents

Notations	xii
1 Introduction	1
1.1 Purpose and scope	2
1.2 Thesis outline	3
2 System overview	5
2.1 Torque estimation	8
3 Estimation of CA50	9
3.1 Heywood's formula for heat release calculations	10
3.2 Calculation of CA50	11
3.3 Evaluation of the method	13
3.4 Engine test cell results	15
4 Pilot detection	17
4.1 Estimation method 1 - pattern recognition	19
4.1.1 Evaluation of estimation method 1	20
4.1.2 Engine test cell results	22
4.2 Estimation method 2 - pressure difference	24
4.2.1 Evaluation of estimation method 2	26
4.2.2 Engine test cell results	28
5 Controller Design	31
5.1 Engine Test Cell Results	35
6 Discussion	39
6.1 Future work	41
7 Conclusion	43
Bibliography	45

Notations

Abbreviations

<i>BDC</i>	Bottom Dead Center	
<i>BSFC</i>	Break Specific Fuel Consumption	
<i>CA50</i>	Crank Angle at 50 % fuel combustion	[deg]
<i>CAD</i>	Crank Angle Degree	
<i>CO</i>	Carbon Oxide	
<i>ECM</i>	Engine Control Module	
<i>EGR</i>	Exhaust Gas Recirculation	
<i>EVO</i>	Exhaust Valve Opening	
<i>GHG</i>	Greenhouse Gas	
<i>GTT</i>	Volvo Group Trucks Technology	
<i>HC</i>	Hydro Carbon	
<i>HR50</i>	Heat release at 50 % fuel combustion	[J]
<i>ICPS</i>	In-Cylinder Pressure Sensor	
<i>IVC</i>	Inlet Valve Closing	
<i>LQ</i>	Linear Quadratic	
<i>MIMO</i>	Multiple Input Multiple Output	
<i>NO_x</i>	Nitrogen Oxides	
<i>PM</i>	Particulate Matter	
<i>TDC</i>	Top Dead Center	

Capital Letters

<i>C</i>	Constant for adiabatic isotropic process	
<i>J</i>	Quadratic cost function	
<i>K</i>	Controller gain matrix	
<i>L</i>	Crank lever function scaled by cylinder area	
<i>N_c</i>	Number of cylinders	
<i>Q_{cr}</i>	Crevice corresponding energy	[J]
<i>Q_{ht}</i>	Convective heat transfer	[J]
<i>Q_n</i>	Net heat release	[J]
<i>Q_{tot}</i>	Gross heat release	[J]
<i>T_g</i>	Indicated torque	[Nm]
<i>V</i>	Cylinder volume	[m ³]
<i>V_c</i>	Clearance volume	[m ³]

Small Letters

a	Crank radius	[m]
b	Cylinder bore	[m]
$conv$	Convolute curve for pilot detection estimation method 1	
f	Reference curve for pilot detection estimation method 1	
l	Length of connecting rod	[m]
n	Number of samples	
p	Cylinder pressure	[Pa]
s	Stroke Length	[m]

Greek Letters

γ	Specific heat ratio	
$ \Theta $	Length of the 4-stroke engine cycle, 720°	
θ	Crank shaft angle relative to TDC	[deg]

Distinguishing marks

$\hat{}$	Approximation or estimate
$\bar{}$	Average value
\sim	Measurement
\mathbf{x}	Thick letter denotes a vector

1

Introduction

Diesel engines are forecasted to be the main motor for trucks in the foreseeable future. Considerable efforts are spent on refining the diesel engine to reduce its environmental impact [1]. The environmental impact of the diesel engine depends on several aspects. Some of these aspects are; reducing the brake specific fuel consumption (BSFC), decreasing emissions and noise from the engine, but also making the engine flexible for biofuels.

The diesel engine, by combustion, contributes to increasing the level of several harmful exhaust gas components as nitrogen oxides (NO_x), hydrocarbons (HC), carbon oxide (CO) and particulate matter (PM), which includes soot. When BSFC and PM emissions are decreased, the emission of NO_x is increased, which means that a suitable compromise has to be made to be able to lower all emissions in an optimal way. In addition, noise emissions come from the diesel engine. If the pressure in the engine is increased rapidly, the noise levels in the engine will rise [2][3].

If the diesel engine is flexible for use of biofuels, the greenhouse gas (GHG) emissions and fossil fuel dependency will decrease. There is, however, some problem with using biofuel instead of petroleum-based fuel. The energy content of biofuels is lower than for regular diesel, which makes the maximum power output from the engine lower. Another problem with biofuels is that, even though most of the emissions are lower, the NO_x emissions are higher, compared to petroleum-based diesel [4].

With increasing demands on reducing the diesel engines environmental impact, the complexity and accuracy of engine control systems become more important. One approach to handle the demands on the engine control system is to make use of combustion control that depends on information about the in-cylinder pressure, using in-cylinder pressure sensors (ICPS) [5][6]. The information obtained by keeping track of each cylinder pressure can be used for feedback control of, for instance, air-fuel ratio, injection patterns and exhaust gas recirculation (EGR) [7].

Making use of in-cylinder combustion control provides several advantages. Accurate evaluation of the combustion events is allowed by evaluating cylinder pressure information. This contributes to a more accurate fuel delivery, more reliable engine operations and enables a reduction of engine emissions. This requires the sensors to be durable with a high accuracy, but to a low cost [5]. To optimize engine operations, ICPS based feedback control is an ideal method. The cylinder pressure can be

used to obtain optimal engine control through manipulation of fuel injections [8][9].

Fuel injections can be divided into three main categories; pilot-, main- and post-injection and there may also be more than one pilot- and/or post-injection. Multiple fuel injections can control the cylinder pressure as well as decrease harmful exhaust gas components. The timing and quantity of the injection are the normally controlled parameters in an engine. These are typically the control parameters when designing an ICPS based feedback controller as well [10].

1.1 Purpose and scope

A method that can reduce the content of harmful exhaust gas components, reduce fuel consumption, and at the same time make the engine flexible for use of biofuels was investigated. For that purpose, a control system was designed to control the combustion by feedback from a sensor that measures the pressure inside one cylinder. The primary task was to manipulate the injections of diesel to be able to control the pressure curve for the cylinder, to get a desired heat release profile. Only one sensor was used to measure the pressure in one of the cylinders. The measured pressure was assumed to be the same for the other five cylinders in the engine.

The injector is able to handle several injections of diesel per cycle. For the main-injection, the timing of the injection was manipulated. The total quantity of fuel was also manipulated, which affects all the three different types of injections. For the pilot-injection, the two methods for pilot detection were investigated, but it was not controlled. This resulted in two control signals in the system; main injection timing and total fuel quantity. The interesting outputs are: crank angle for 50 % heat release after top dead center (TDC), which is denoted CA50, and the average indicated torque, which was estimated from the pressure. This makes the system a multiple input multiple output (MIMO) system with two control signals and two output signals.

The control structure used was a linear quadratic (LQ) controller. To create the state space model, the injections of diesel were related to the estimated outputs. The above methods and control structure were implemented and modeled in `Targetlink`.

1.2 Thesis outline

The second chapter of the thesis gives an overview, both of the diesel engine, the signals available from the engine, general problems, and the torque estimation. The third chapter presents the method used for estimating CA50 and the results from simulation and engine tests. The fourth chapter presents the two different methods for pilot detection, together with the results from simulation and engine tests. The fifth chapter contains the development and implementation of the LQ MIMO control structure and also the results from engine tests. These chapters are followed by a discussion about the results and finally, conclusions are presented.

2

System overview

The four-stroke diesel engine is the most common engine used in trucks. One cycle in one cylinder consists of two crankshaft revolutions, where four separate strokes are running. The engine used in this project has six cylinders, where the cylinders operate simultaneously. The four strokes are demonstrated in Figure 2.1.

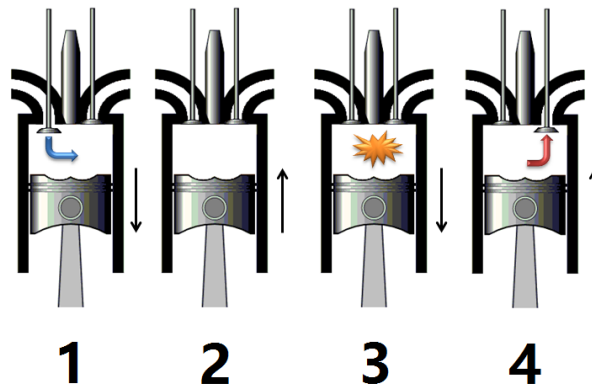


Figure 2.1: The four strokes, intake, compression, power, and exhaust, of an engine cycle [11].

The first stroke of an engine cycle, to the left in Figure 2.1, is called the intake stroke. The piston begins at TDC with the inlet valve open, moving downwards and at the same time, fresh air is pressed into the cylinder. When the piston has reached bottom dead center (BDC), the inlet valve is closed (IVC) and the first stroke is done. The second stroke is called the compression stroke. At this stage, both the inlet valve and exhaust valve are closed, and the piston is moving upwards to compress the air. At the end of this stroke, the pressure is increasing faster, because of the injection of fuel.

When the piston reaches TDC, the third stroke begins, called the power stroke. The fuel is ignited by the high temperature and pressure. This pushes the piston down towards BDC and the crank starts to rotate. The last stroke is called the

exhaust stroke. The exhaust valve is opened (EVO) and the remaining gases leave the cylinder as the piston moves towards TDC [2].

To recognize the relationship between the crankshaft and the piston, a cross-section is displayed in Figure 2.2.

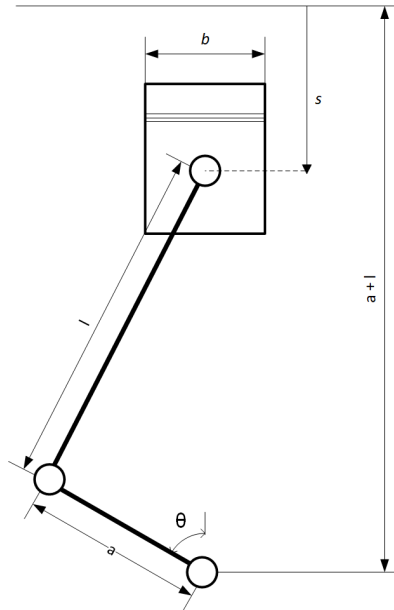


Figure 2.2: Relation between crankshaft and piston [6].

In Figure 2.2, θ is the crankshaft angle, l is the length of the connecting rod, a is the crank radius, s is the stroke length, and b is the cylinder bore.

The data needed from the engine is the pressure and crankshaft angle. The pressure data used in this project is received from a piezoelectric pressure sensor, and is sampled with the sampling interval of 1° and 6° . A problem with this kind of sensor is that it drifts over time.

To compensate for the drift of the pressure sensor, a simple moving average filter is implemented. This filter determines the difference between the pressure and boost pressure at 180° before TDC, when the inlet valve is still open. The pressure and the boost pressure should, at this point, be the same which makes it possible to determine if there is any drift in the sensor. This is done one time per cycle, and to avoid cycle-to-cycle variations, the filter calculates a mean of six cycles. The mean is then added to every measurement in the pressure vector [6].

To get information about the crankshaft location, an angular measurement sensor is used. The flywheel has a tooth every 6° and is separated by gaps every 120° . The sensor is able to determine the crankshaft angle by measuring discrete points at each tooth and deliver a vector of measurements to the engine control module (ECM) every 120° . When the vector has been delivered, a new measurement is initialized. With this approach, the sampling interval will be 6° .

To achieve a shorter sampling interval of 1° , another approach is required. Due to

limitations in the hardware, a few problems need to be solved. The first problem with a higher sampling interval is that it takes some time for the ECM to set up the new measurement, which will result in loss of values at the beginning of the measurement. The vector will result in a shifted vector, where the first measurement that is done is placed at the beginning of the vector, and the lost values are represented by zeros in the end.

Another problem is that the measured pressure may have a TDC-offset. When the engine is motored, i.e. no combustion, the pressure should have its peak approximately in TDC. If this is not the case, there is an offset called TDC-offset.

To solve the problems with the lost values and the TDC-offset, a function is implemented to handle this. First, the number of values in each vector that are lost are counted. The vector is then shifted to remove the TDC-offset. When a complete cycle is obtained, linear interpolation is done to smooth the pressure where the values are missing. The effect of the interpolation can be seen in Figure 2.3.

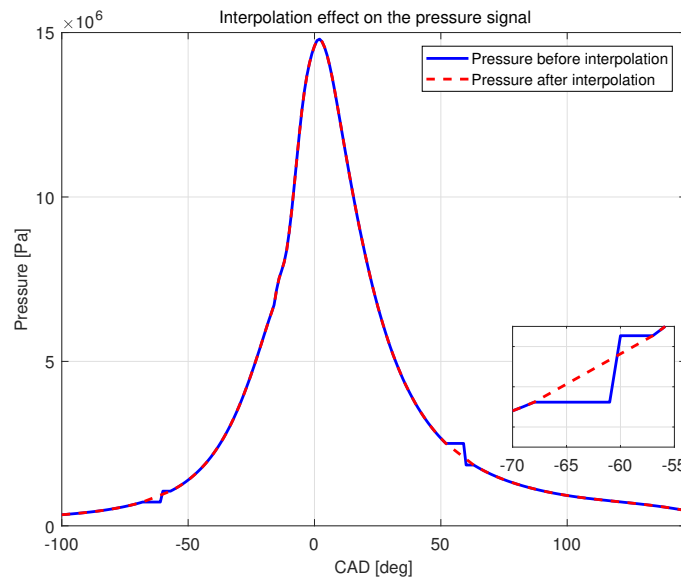


Figure 2.3: Interpolation of the pressure signal.

2.1 Torque estimation

The estimation of the torque is taken from the thesis work "Torque estimation from the in-cylinder pressure sensor for closed-loop torque control" [6]. The estimation method uses one in-cylinder pressure sensor to estimate the average indicated torque through a Riemann middle sum. With some approximations and simplifications, for example, to set the pressure inside the crankcase equal to the atmospheric pressure, the average indicated torque can be determined as

$$\bar{T}_g = \frac{N_c}{|\Theta|} \int_{\Theta} L(\theta) p_x(\theta) d\theta, \quad (2.1)$$

where N_c is the number of cylinders in the engine, Θ is the engine cycle of a four-stroke engine with $|\Theta| = 720^\circ$ as the length of a cycle, $p_x(\theta)$ is the pressure in the combustion chamber and $L(\theta)$ describes how the pressure on the piston generates torque on the crankshaft. Since the pressure signal is sampled with a constant sampling interval and delivered to the process in vectors every 120 crank angle degree (CAD), there is a pressure signal with equidistant points available and the approximation can be expressed as

$$\bar{T}_g \approx \hat{T}_g = N_c \frac{1}{n} \sum_{i=0}^{n-1} L(\theta_i) \tilde{p}(\theta_i), \quad (2.2)$$

where n is the number of samples and $\theta_i = (2i + 1) \frac{|\Theta|}{2n}$. Since the number of samples (n) and the crank angle degrees (θ_i) can be predetermined, the first part of the equation ($\frac{N_c}{n} L(\theta_i)$) can be calculated in advance, giving the column vector $\mathbf{L} := \frac{N_c}{n} L(\theta_I)$, where $\theta_I := \{\theta_i : i = 1, \dots, n\}$. The average indicated torque is then computed through the scalar product

$$\hat{T}_g = \mathbf{L}^T \tilde{\mathbf{p}}, \quad (2.3)$$

with $\tilde{\mathbf{p}} := \tilde{p}(\theta_I)$ as the incoming vector of pressure measurements. From now on, \bar{T}_g will be denoted T .

The estimation of the torque was done with a sampling interval of 6° , since it was concluded in the thesis work that this was enough to get a good estimation [6].

3

Estimation of CA50

CA50 is a measurement of when, in terms of CAD, 50 % of the fuel has burnt over one engine cycle. Accurate estimation of CA50 contributes with essential information about the combustion process, which can be used for improving the performance of an engine [12]. An optimum value of CA50, in terms of optimal engine efficiency, is around 8 CAD after TDC [13].

The interesting interval when estimating CA50 is between IVC and EVO, since this is when the fuel is burning, i.e. when the heat is released. An approximation of CA50 could therefore be made based on a vector of cylinder pressure measurements between these two points.

The derivation of the heat release can be done in numerous ways. A summer internship made in 2017 at GTT investigated a couple of different methods [14]. The conclusion was that the least complex method, Heywood formula method, yielded a satisfying result. CA50 can be estimated by deriving the heat release profile and find where the curve reaches 50% of its peak. The method contains several steps. First, the apparent net heat release rate is derived using the Heywood formula method [2]. The heat release rate is then integrated to find the desired heat release curve. Finally, the CA50 measurement is estimated from the derived curve.

3.1 Heywood's formula for heat release calculations

Heywood's formula for heat release calculations takes advantage of the first law of thermodynamics, and assumes that the work environment is quasi-static [2]. The total heat release is calculated by the following equation:

$$\frac{dQ_{tot}}{d\theta} = \frac{\gamma}{\gamma - 1} p \frac{dV}{d\theta} + \frac{1}{\gamma - 1} V \frac{dp}{d\theta} + \frac{dQ_{ht}}{d\theta} + \frac{dQ_{cr}}{d\theta}, \quad (3.1)$$

where Q_{tot} is the gross heat release, γ is the ratio of specific heat, modeled as a constant with a value of 1.3971, Q_{ht} is the convective heat transfer, Q_{cr} is the crevice corresponding energy, created by gas flowing into e.g. the area between the piston, the piston rings, and the cylinder wall, and V is the cylinder volume. The cylinder volume is calculated through:

$$V = V_c + \frac{\pi b^2}{4} (l + a - a \cos(\theta) + \sqrt{l^2 - a^2 \sin^2(\theta)}), \quad (3.2)$$

where V_c is the clearance volume, l is the length of the connecting rod, a is the crank radius and b is the cylinder bore.

The convective heat transfer and crevice corresponding energy are only a small fraction of the fuel energy and affect the heat release the most at the end of the combustion process. The slope of the heat release will be almost as steep, with as without, the convective heat transfer and crevice corresponding energy included. This means that it is enough to look at the apparent net heat release to estimate a proper value of CA50. The apparent net heat release rate is calculated as the difference between the heat transfer rate through the walls and the apparent gross heat release rate, i.e.

$$\frac{dQ_n}{d\theta} = \frac{\gamma}{\gamma - 1} p \frac{dV}{d\theta} + \frac{1}{\gamma - 1} V \frac{dp}{d\theta}, \quad (3.3)$$

where Q_n is the apparent net heat release [2].

3.2 Calculation of CA50

The apparent net heat release is obtained by integrating the apparent net heat release rate. To calculate the CA50 point, the first step is to find the value where 50 % of the fuel has burnt off (HR50). The HR50 value is calculated by the following equation:

$$HR50 = 0.5 \max(Q_n). \quad (3.4)$$

By rewriting Equation (3.4) to

$$HRx = \frac{x}{100} \max(Q_n), \quad (3.5)$$

where x represents the derived percent of fuel burnt, and then uses the same method as above, it is possible to find other CA-points.

Since the pressure is sampled with a certain frequency, it is likely that the calculated HR50 value does not exist in the Q_n -vector. For this reason, CA50 is found by first finding the two indices in the Q_n -vector that generates heat release values closest to the HR50 value. These indices are subsequently used to extract values from both the θ - and Q_n -vector. To minimize the error caused by the sampling interval, linear interpolation is applied between the previously mentioned values of θ and Q_n according to

$$P_n(x) = c_0 + c_1(x - x_1), \quad (3.6)$$

which in this case means

$$\begin{aligned} HR50 &= c_0 + c_1(CA50 - CA50_{\text{low}}) \\ c_0 &= HR50_{\text{low}} \\ c_1 &= \frac{HR50_{\text{high}} - HR50_{\text{low}}}{CA50_{\text{high}} - CA50_{\text{low}}} \end{aligned} \quad (3.7)$$

which gives

$$CA50 = \frac{HR50 - c_0}{c_1} + CA50_{\text{low}}, \quad (3.8)$$

where low denotes the first values of CA50 and HR50 and high denotes the next value of CA50 and HR50. The interpolation can be seen in Figure 3.1 where the sampling interval is 1° and Figure 3.2, where the sampling interval is 6° .

3. Estimation of CA50

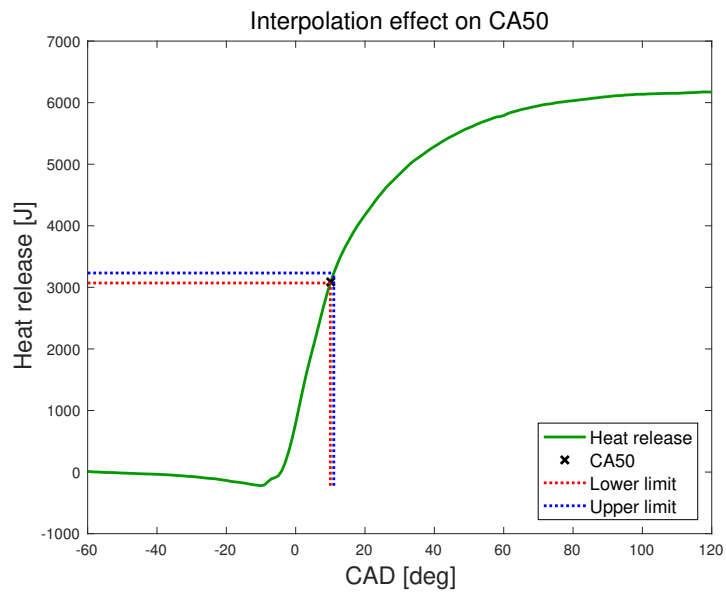


Figure 3.1: Interpolation with sampling interval = 1° .

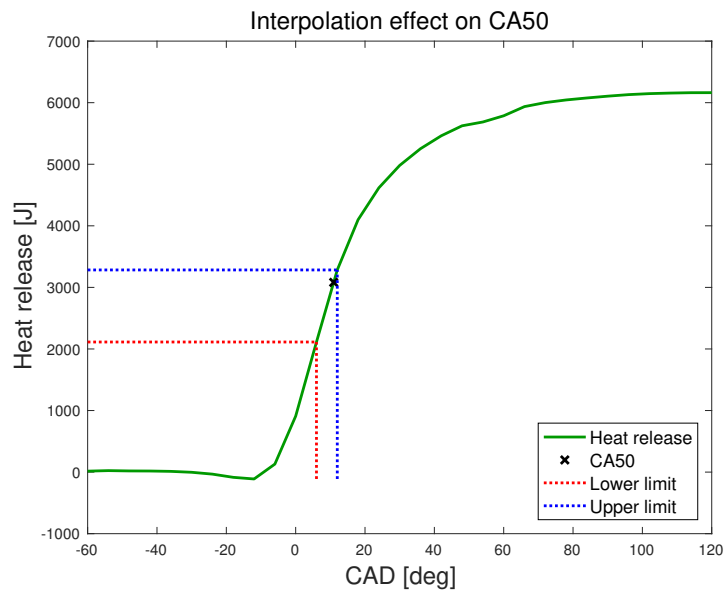


Figure 3.2: Interpolation with sampling interval = 6° .

3.3 Evaluation of the method

The method was modeled in `Targetlink` and tested in simulation at different operating points (see Table 3.1). The data that was used was collected from an engine test cell, and has been filtered to have no lost values and hardly no noise. All available cases have one pilot injection and one main injection.

Case	RPM	Nm
1	800	1800
2	900	2100
3	1100	1800
4	1200	2100
5	1300	2100
6	1600	2350
7	1800	2650

Table 3.1: Operating points for simulation.

Results from the simulations are displayed in Figure 3.3 and 3.4, where each estimate is a mean from 50 cycles.

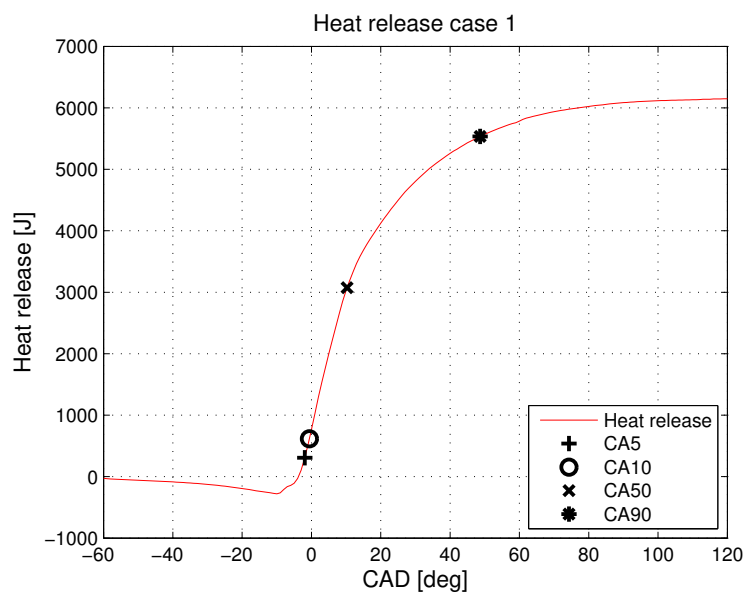


Figure 3.3: Heat release over CAD where CA50=9.98°, case 1.

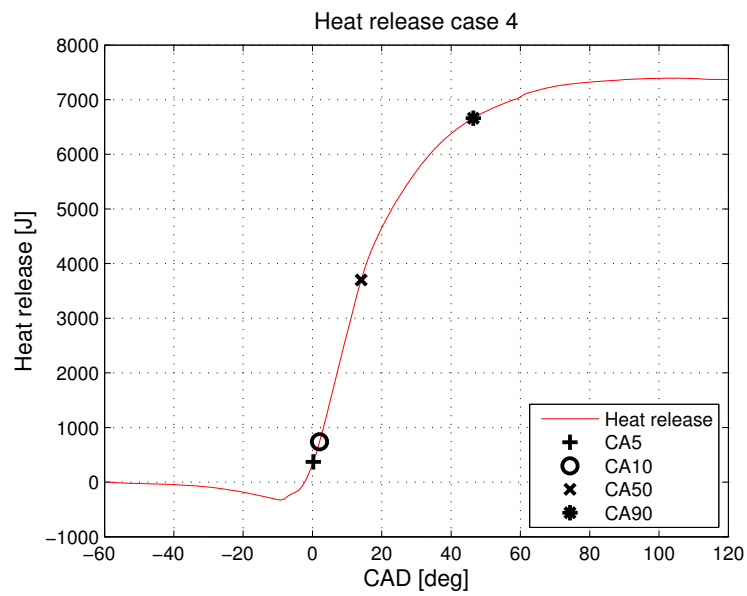


Figure 3.4: Heat release over CAD where $CA50 = 13.56^\circ$, case 4.

When observing the results, one can see that the estimates of the different CA-points are reasonable, since in all cases CA50 is located close to the optimum value.

3.4 Engine test cell results

The engine tests were performed on several different engines with various specifications on for example, the volume of the engine and internal mechanics. The results from the engine tests can be seen in Figure 3.5, 3.6, and 3.7.

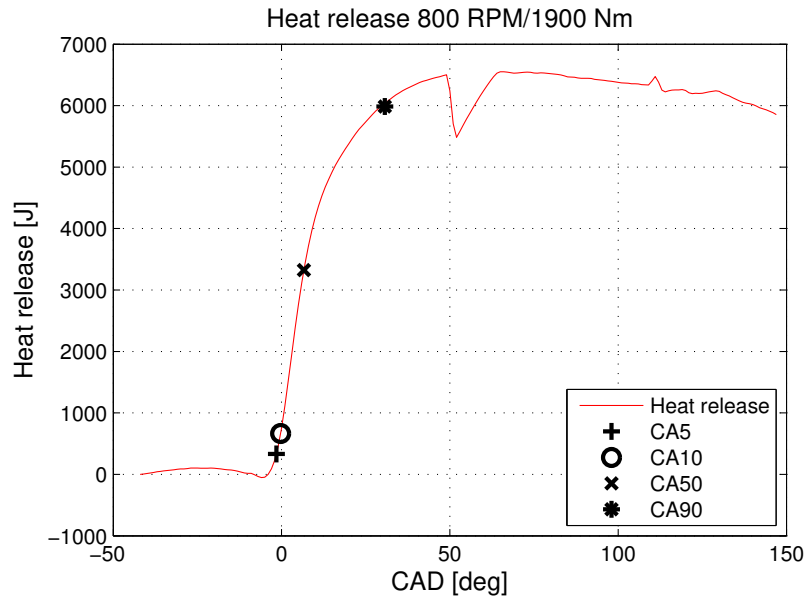


Figure 3.5: Heat release over CAD where $CA_{50} = 6.59^\circ$.

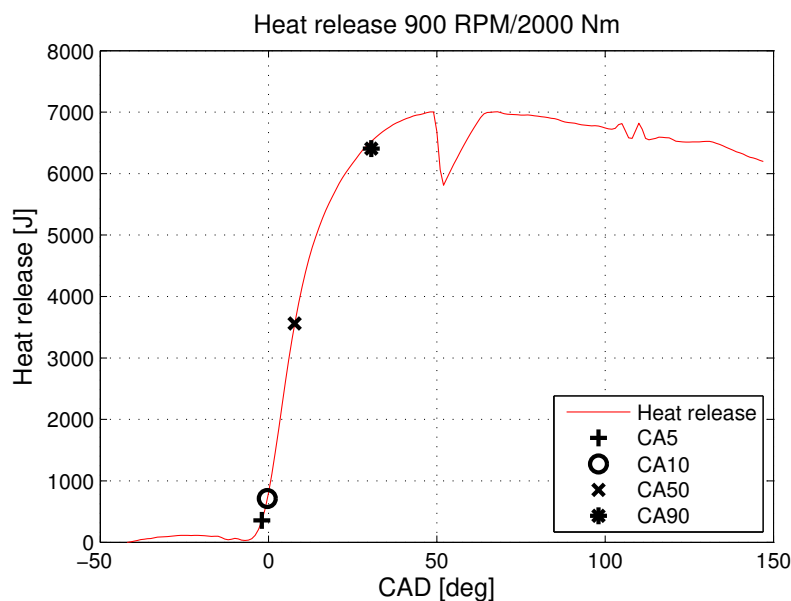


Figure 3.6: Heat release over CAD where $CA_{50} = 7.76^\circ$.

When observing Figure 3.5 and 3.6 it is visible that the results are similar to the results from simulations. One notable difference is that the effect of the interpolation can be seen at around 50 CAD. However, since the calculations of the different CA-point are calculated through the maximum value of the heat release, this will not

3. Estimation of CA50

affect the actual values of the different CA-points. Also in engine tests, CA50 is located around the optimum value. There was a program in the test cell showing the different CA-point, which the estimates were compared to, called AVL IndiCom indicating software. The estimates were close to the IndiCom values, within about ± 1 CAD difference. The IndiCom values were not saved.

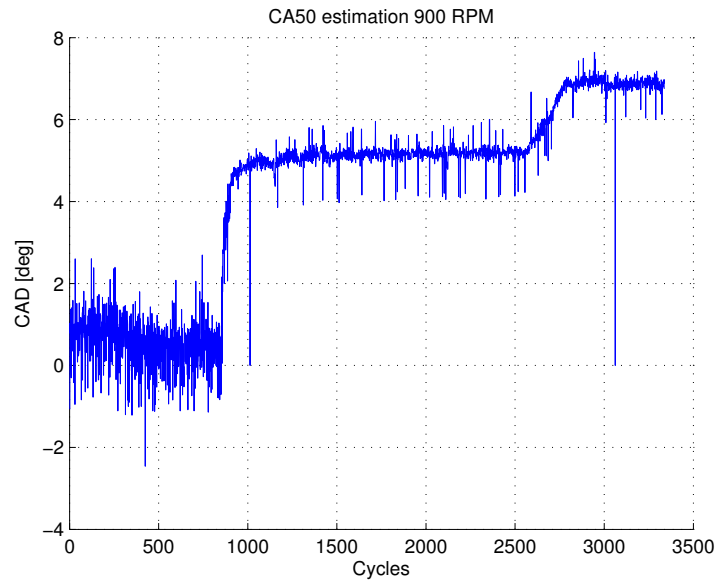


Figure 3.7: CA50 over cycles at 900 RPM with different torques; Cycles = [0:850] T= 350 Nm, Cycles = [850:2500] T= 1200 Nm, Cycles = [2500:3300] T=2000 Nm.

One interesting result is that the estimate of CA50 is noisier at lower torque values (see Figure 3.7). When the torque is 350 Nm, CA50 has an interval around 3 CAD, while at higher torques the interval is around 2 CAD and with fewer outliers.

4

Pilot detection

The number of injections given to the engine during one engine cycle depends on the desired behavior from the engine. A pilot injection is given before the main injection and is primarily used to reduce noise and emissions. The quantity and timing of the pilot injection have large variations depending on which system it is applied to, but small quantities of the pilot injection are preferable [10]. The sampling interval has a substantial impact on the possibility to estimate the heat release from a pilot injection, as can be seen in Figure 4.1.

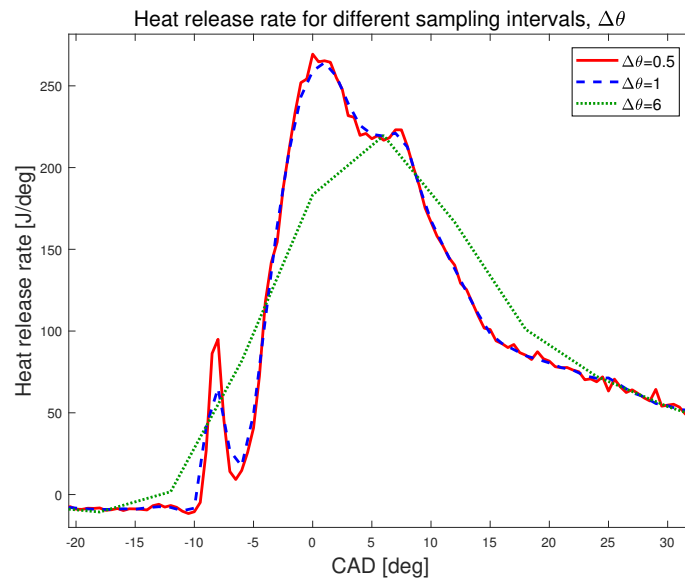


Figure 4.1: Heat release rate for different sampling intervals ($\Delta\theta$).

The heat released from an injection can be detected when the heat release rate peaks. If the heat release rate contains more than one peak, another injection can be detected. As can be seen in Figure 4.1, the heat release rate contains two peaks; first one smaller that stems from the pilot injection, followed by a larger that stems from the main injection. It is also clear that the pilot injection is not always possible to detect. When the sampling interval is 6° , the pilot injection may be undetectable. When the sampling interval is 1° , the pilot injection is detectable. However, compared to the sampling interval of 0.5° , it can be seen that the observed heat released from the pilot injection is not as high. This means that the sampling

4. Pilot detection

interval has a substantial impact on the possibility to correctly determine the value of the heat released.

Since the data available in this project only have the sampling intervals 1° and 6° , it is only possible to implement a detection of the pilot injection and not estimate the heat released from the pilot injection. The output is thus boolean, returning true if a pilot injection has been detected, and false if no pilot injection has been detected. If it is detectable if a pilot injections has been made or not, it is possible to alter the quantity of the pilot injection to ensure that it burns, and thus decreasing noise emissions.

4.1 Estimation method 1 - pattern recognition

When observing the derivative of the heat release rate (ddQ), it can be seen that the pilot injection makes a specific pattern. If a pilot injection is made, the curve is formed like a sinusoidal around the angles where it is made. If the pilot injection is not made, the result is a straight line instead. In the first estimation method, this observation is exploited. First, a reference curve f was created, to resemble this behavior (see Figure 4.2). This was done by calculating a mean curve from 50 cycles of ddQ .

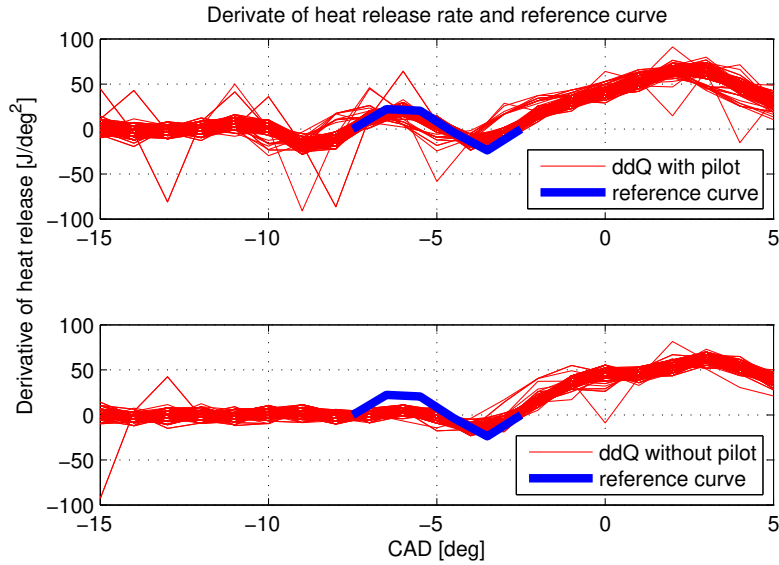


Figure 4.2: Derivative of the heat release rate, with and without pilot together with the reference curve.

The reference curve was convoluted with the derivative of the heat release rate to see if the specific behavior that a pilot injection gives, appears somewhere in a limited window, j . This was done according to standard convolution

$$\text{conv}_j = \sum_i f_i * ddQ_{i+j-1}, \quad (4.1)$$

where i is the length of the reference curve and conv is the convoluted curve with length j . After the convolution was done, the maximum value of the conv is compared to a threshold, which is determined through examine the maximum value of conv for different operating points. If the maximum value of conv is larger than the threshold, a pilot injection is considered detected.

4.1.1 Evaluation of estimation method 1

The modeled pilot detection method was tested on data collected from the engine test cell. The results can be seen in Figure 4.3 and 4.4.

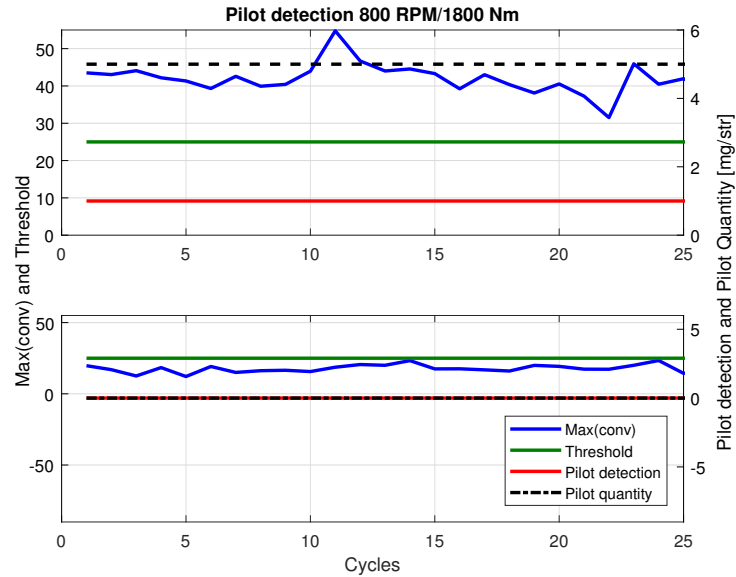


Figure 4.3: Pilot detection for method 1 at the operating point 800 *RPM*/1800 *Nm*.

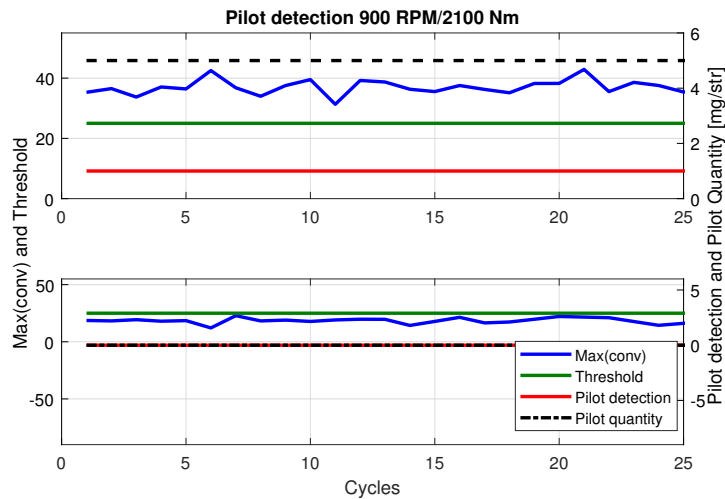


Figure 4.4: Pilot detection for method 1 at the operating point 900 *RPM*/2100 *Nm*.

Figure 4.3 displays the maximum value of the convoluted curve, together with the threshold for pilot detection, the pilot detection, and the pilot quantity when the pilot is on (sub figure above) and off (sub figure below) in the operating point 800 *RPM*/1800 *Nm*. When the pilot quantity is 0 *mg/str* it means that there is no

pilot injection to the engine. It can be seen that when there is a pilot injection, the maximum of the convoluted curve is located above the threshold, which indicates a pilot injection, and the pilot detection will be true (=1). When the quantity of the pilot injection is 0 *mg/str*, the maximum of the convoluted curve is located below the threshold, which delivers a false value of the pilot detection (=0). The same behavior can be seen in Figure 4.4, which illustrates the same measurements as Figure 4.3 but for the operating point *900RPM/2100Nm*.

4.1.2 Engine test cell results

The results from the engine tests can be seen in Figure 4.5 and 4.6.

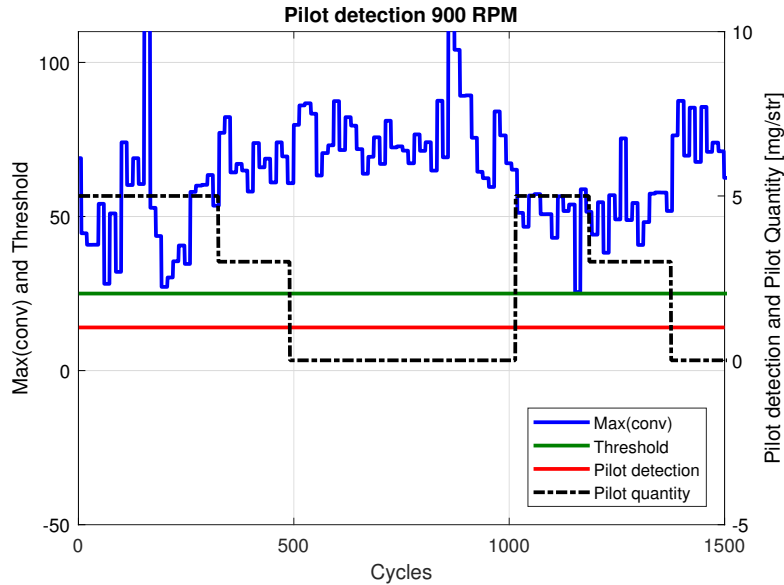


Figure 4.5: Pilot detection for method 1 at the operating point 900 *RPM* with different torque values.

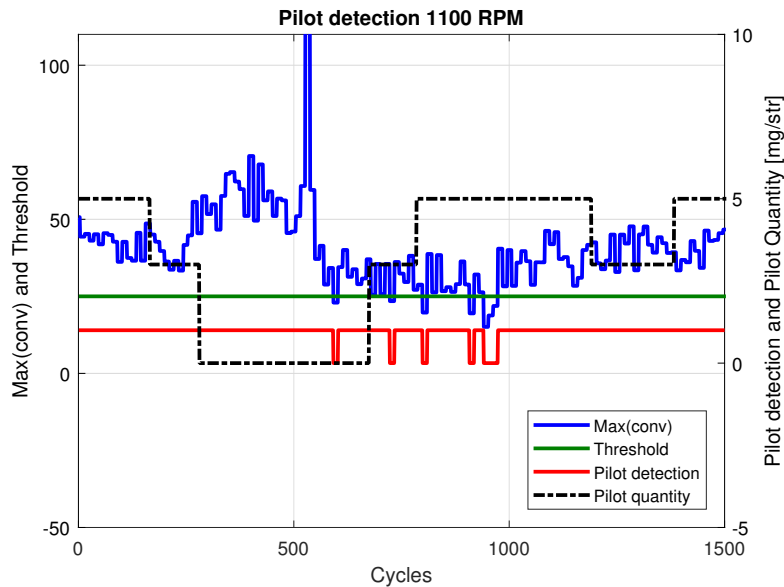


Figure 4.6: Pilot detection for method 1 at the operating point 1100 *RPM* with different torque values.

Figure 4.5 illustrates the same measurements as in the simulation results, but the operating point is 900 *RPM* with different values on the torque. The method was tested by giving a pilot quantity of 5 *mg/str*, 3 *mg/str* and 0 *mg/str* for each torque value. It can be seen that the maximum of the convoluted curve is more noisy, compared to when the method was evaluated, which is an effect of a noisy

ddQ (see Figure 4.7). The value is constantly located above the threshold which results in a constant pilot detection, even when the quantity of the pilot injection is 0 mg/str . Similar results can be seen in Figure 4.6, with the difference that the pilot detection is false in some cycles, but both when the quantity of the pilot injection is 5 mg/str , 3 mg/str and 0 mg/str .

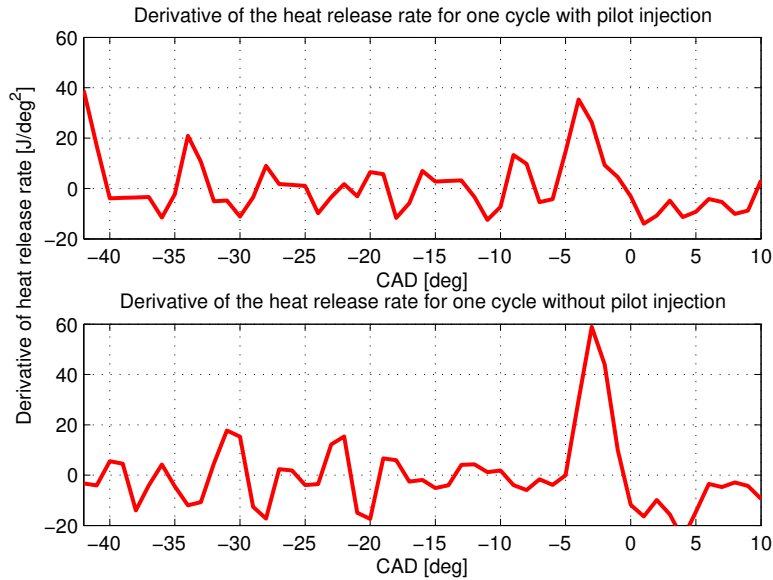


Figure 4.7: Derivative of the heat release rate with and without pilot injection for one cycle.

In Figure 4.7 it can be seen that the noise has a similar shape compared to the effect of the pilot injection, which also means that the shape is similar to the reference curve. The effect from the pilot injection should be displayed between -15 and -5 CAD, and in this interval, this is displayed when a pilot injection exists, but not when there is no pilot injection.

4.2 Estimation method 2 - pressure difference

The second method examines the pressure between the start of the pilot injection and the start of the main injection. As can be seen in Figure 4.8, the pressure is slightly higher when a pilot injection has been made.

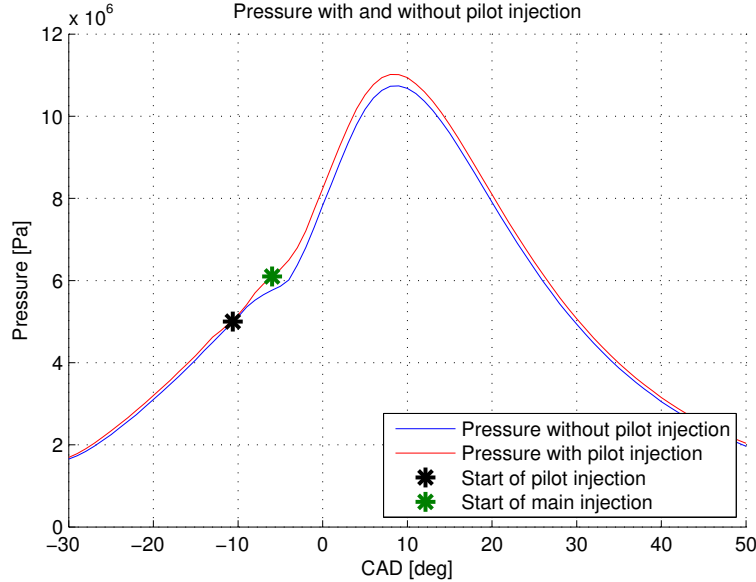


Figure 4.8: Pressure with and without pilot injection.

By making use of adiabatic isentropic processes it is possible to estimate how the pressure curve will look like without any injections. This can then be used as a reference [2]. An adiabatic isentropic process is an ideal thermodynamic process, where heat transfer is not included. The process can be summarized to

$$p_k V_k^\gamma = C_k, \quad (4.2)$$

where C is a constant and k is at which CAD the process is performed. By applying the equation at the same CAD that the pilot injection is made, θ_p , a constant C_{ref} is obtained, which is used to calculate the reference pressure curve. The reference pressure curve, p_{ref} , is calculated through Equation (4.2), in a window between the start of pilot injection and the start of the main injection, θ_m , resulting in a vector with the same size as the window. This is done for every cycle in real time.

The next step is to integrate the difference between the measured pressure and the reference according to

$$p_{diff} = \int_{\theta_p}^{\theta_m} (p_{measured} - p_{ref}) d\theta, \quad (4.3)$$

where $p_{measured}$ is the measured pressure and p_{diff} represent the integrated difference. The difference is compared to a threshold to determine if a pilot injection

has occurred or not. When p_{diff} is larger than the threshold, it is interpreted as a pilot injection has occurred. To avoid error detection, a mean from ten cycles is calculated and if a pilot injection is detected more than, for example, 70% of the cycles, the pilot detection signal will be considered true.

4.2.1 Evaluation of estimation method 2

Also for this method, evaluation was done with data from the test cell. The results can be seen in Figure 4.9 and 4.10.

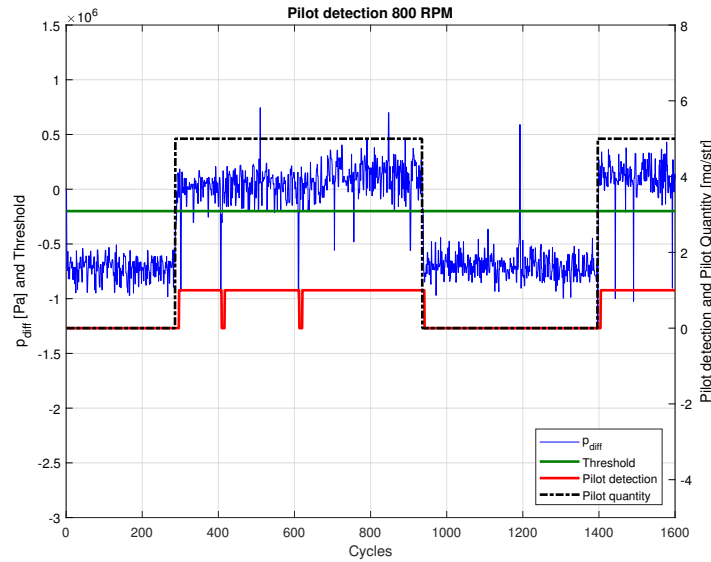


Figure 4.9: Pressure difference, together with pilot quantity, pilot detection, and the threshold at $-2 \times 10^5 Pa$ at the operating point 800 RPM, with different torque values.

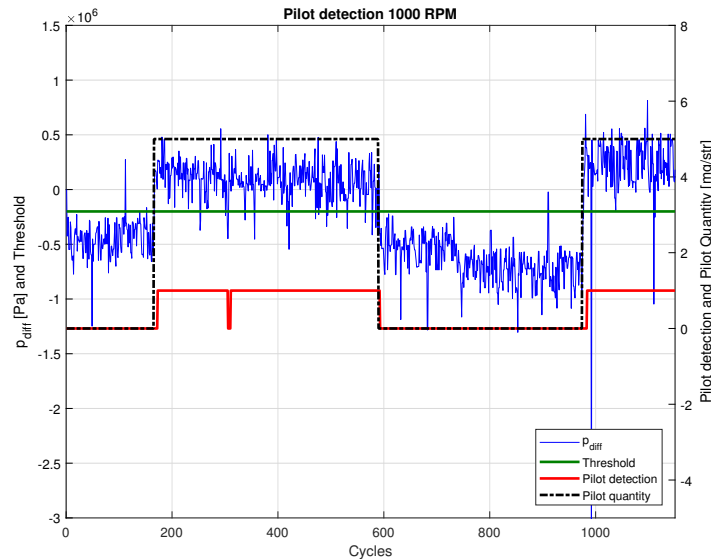


Figure 4.10: Pressure difference, together with pilot quantity, pilot detection, and the threshold at $-2 \times 10^5 Pa$ at the operating point 800 RPM, with different torque values.

It can be seen from both figures that the estimation method works well. There are only two false detections when the engine speed is 900 RPM and one false detection

when the engine speed is 1000 *RPM*. It is also clear that a delay exists when the quantity of the pilot injection change. This is due to the fact that the pilot detection is calculated from a mean over ten cycles.

4.2.2 Engine test cell results

The results from the engine tests can be seen in Figure 4.11, 4.12, and 4.13.

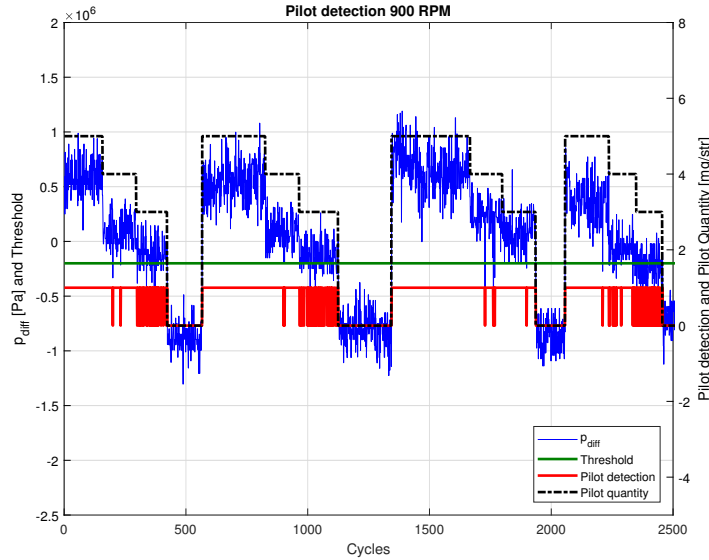


Figure 4.11: Pressure difference, together with pilot quantity, pilot detection, and the threshold at $-2 \times 10^5 Pa$ at the operating point 900 RPM, with different torque values.

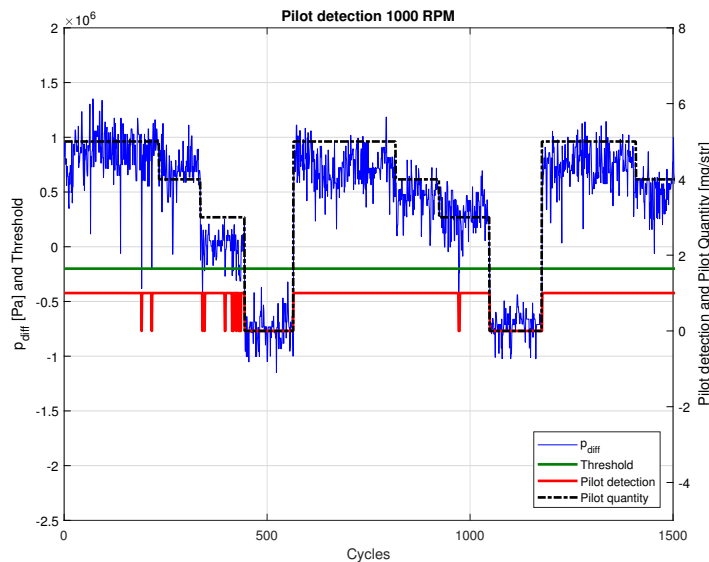


Figure 4.12: Pressure difference, together with pilot quantity, pilot detection, and the threshold at $-2 \times 10^5 Pa$ at the operating point 1000 RPM, with different torque values.

Both when the engine speed is 900 RPM and 1000 RPM, the quantity of the pilot injection is 5, 4, 3, or 0 mg/str, tested at different torques. It can be seen that the estimation works well when the quantity of the pilot injection is either 5 or 0

mg/str . It can also be seen that smaller quantities are detected easier when the engine speed is higher. At $900\ RPM$, almost every pilot detection is wrong when the quantity of the pilot injection is $3\ mg/str$, while at $1000\ RPM$ there are still many outliers, but not as many.

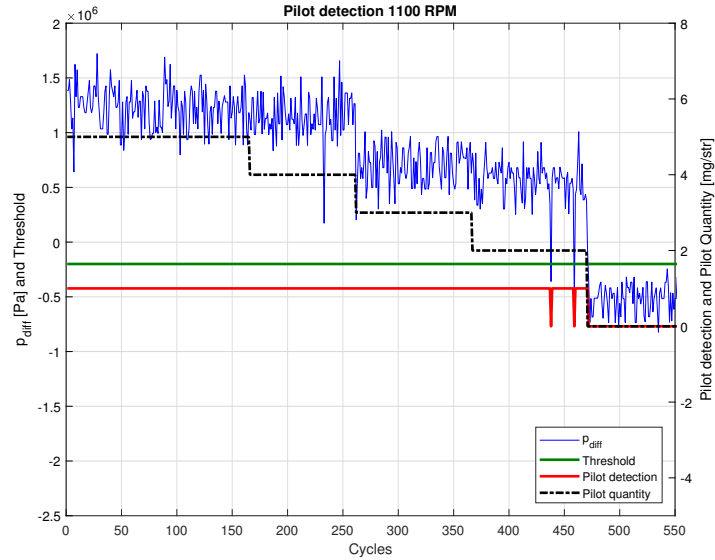


Figure 4.13: Pressure difference, together with pilot quantity, pilot detection, and the threshold at $-2 * 10^5\ Pa$ at the operating point $1100\ RPM/1200\ Nm$.

When the engine speed was $1100\ RPM$ the quantity of the pilot injection was tested at $5, 4, 3, 2,$ and $0\ mg/str$. Here it can be seen that the estimation is correct at a quantity of $5, 4, 3,$ and $0\ mg/str$, and only gives a few fault detection when the quantity is $2\ mg/str$.

5

Controller Design

The objective with the regulator is to control CA50, torque, and the heat release of the pilot injection. This is done by manipulations of main injection timing, the total quantity of fuel given to the engine each cycle, and the quantity of pilot injection. Since the sampling interval of the measured pressure is not short enough, the actual heat release from the pilot injection is not estimated, but detected. The detection will thus result in a boolean signal and will not be included in the MIMO control structure.

One way to manipulate the pilot injection is to implement an if-controller. The controller will check if a pilot injection is detected, and if not, the quantity of the injection will be increased. This procedure will iterate until a pilot injection is detected and will then stop increasing the fuel quantity. However, this control structure was not implemented and tested.

The chosen MIMO control structure is an LQ controller. An LQ-controller minimize the quadratic cost function

$$J = \sum x^T Q x + u^T R u \quad (5.1)$$

where x is the states, u is the control signals, and Q and R are the cost function weights, describing how much the states and inputs contribute to the total cost. This is done by calculating an optimal gain matrix K to get a state-feedback law u_k that minimizes the cost function [15].

$$K = (B^T P B + R)^{-1} B^T P A, \quad (5.2)$$

$$u_k = -K x_k, \quad (5.3)$$

where A and B comes from the discrete time state space model and P is calculated through the discrete-time algebraic Riccati equation

$$A^T P A - P - A^T P B (B^T P B + R)^{-1} B^T P A + Q = 0. \quad (5.4)$$

The first step is to determine the relation between the inputs and outputs to the controller to design the state space model of the control system. The state space model has the following form

$$x_{k+1} = \begin{bmatrix} A_{11} & A_{12} \\ A_{21} & A_{22} \end{bmatrix} x_k + \begin{bmatrix} B_{11} & B_{12} \\ B_{21} & B_{22} \end{bmatrix} u_k$$

where the states $x = [CA50 \ T]^T$, and the are control signals $u = [\Delta\theta_m \ \Delta q_{tot}] = \Delta u$ which is the difference in u for time step k and $k - 1$, i.e. $\Delta u = u_k - u_{k-1}$. The state space matrices were found through trial and error parameter identification. It was concluded that the A-matrix is the identity matrix, meaning that $CA50_{k+1}$ depends on $CA50_k$ and not on the torque and vice verse. This means that a change in the control signal will give a scaled change in the states, i.e. $\Delta x = B\Delta u$. The effect from the parameter values in the B-matrix can be seen in Figure 5.1 and 5.2.

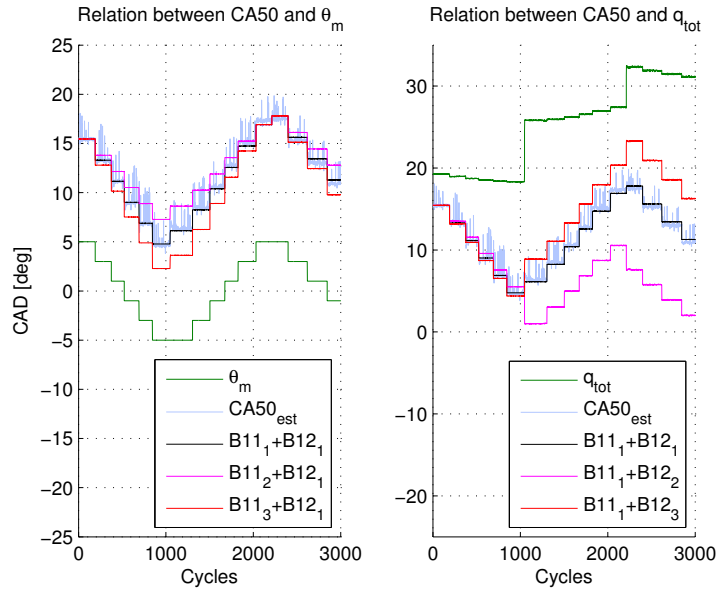


Figure 5.1: Parameter identification to find B11 and B12, where θ_m and q_{tot} has been scaled for easier comparison.

In Figure 5.1 the parameter identification for the first row in the B-matrix is displayed, with different combinations of parameter values. In the figure, θ_m is the requested timing of the main injection, q_{tot} is the requested total fuel quantity, and $CA50_{est}$ is the estimated CA50 from the estimation method in Chapter 3. The remaining curves are the controller estimations of CA50, i.e. $B11+B12$ means $CA50_{k+1} = CA50_k + B11\Delta\theta + B12 \Delta q_{tot}$.

When finding the relation between CA50 and θ_m , B12 was set to a constant value ($B12_1$), while B11 was tested with three different values ($B11_1$, $B11_2$, and $B11_3$). The same was done, but with a constant B11 and varying B12, when finding the relation between CA50 and q_{tot} . It can be seen that CA50 is affected by both the timing of the main injection and the total quantity of fuel injected. Further, it can

be seen that the dependence of the timing of the main injection is stronger than the dependence of the total quantity of fuel, since the shape of θ_m and CA50 is almost identical. However, it can be seen that there is a relation between CA50 and the total amount of fuel as well. This is especially visible around 1000 cycles, where θ_m is constant, but CA50 is slightly increased because of the increase in q_{tot} .

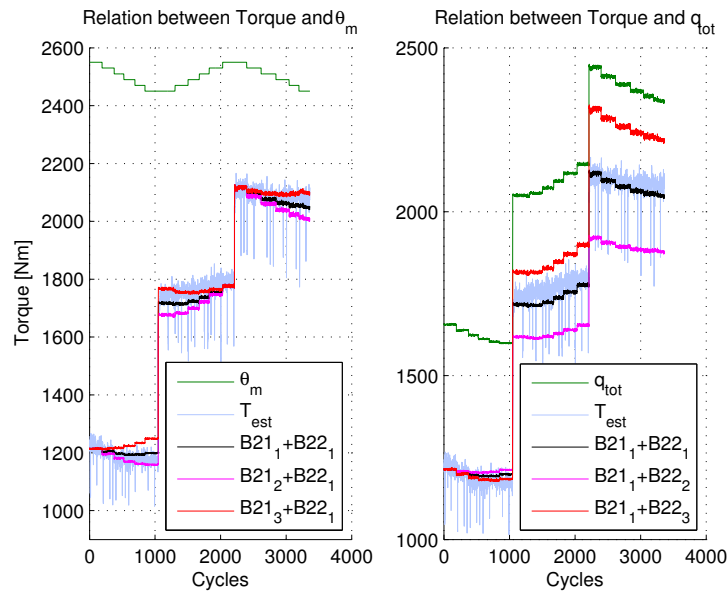


Figure 5.2: Parameter identification to find B21 and B22, where θ_m and q_{tot} has been scaled for easier comparison.

The parameter identification for the second row in the B-matrix is displayed in Figure 5.2, with different combinations of parameter values. The same methodology applies here as in Figure 5.1. When finding the relation between T and θ_m , B22 was kept constant, with different values of B21, and the other way around when finding the relation between T and q_{tot} . In this figure, it can be seen that also the torque has dependencies on both the timing of the main injection and the total amount of fuel injected. The torque depends strongly on the quantity of fuel injected, which can be seen since the shape of T and q_{tot} is similar. In a comparable way that CA50 relates to q_{tot} , T also relates to θ_m .

Implementation of the control system was the next step of the design, and was done according to Figure 5.3. A moving average filter was implemented on both the reference and estimated signals to prevent the effect of cycle-to-cycle variations on the control signals.

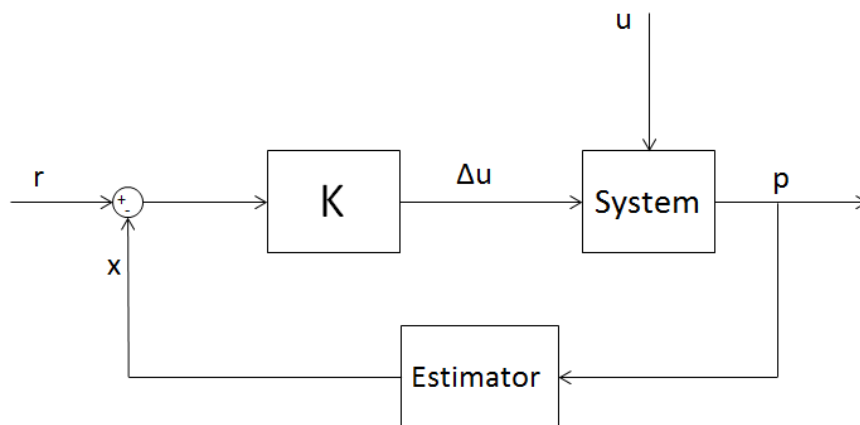


Figure 5.3: Illustration of the control structure

As can be seen in Figure 5.3, the output from the controller is Δu which indicates how much the timing of the main injection and the total amount of fuel should be changed. The output is added to a predefined value for the specific operating point in the system to get the new main injection timing and quantity of fuel.

The controller was implemented, and the behavior was tested in simulation. It was not possible to control the states since a model that relates the control signals to the pressure was not available. Due to this, it was not possible to evaluate the controller in simulation, only to confirm that the control signals seemed reasonable.

5.1 Engine Test Cell Results

Since it was not possible to evaluate the complete controller in simulation, the tuning of the cost function weights Q and R had to be done in the engine test cell. By trial and error, it was concluded that a high penalty on the error i.e. a high value on Q , and a relatively low penalty on the control signals i.e. a low value on R , represent the combination that resulted in the most accurate controller.

The results from the testing of the controller can be seen in Figure 5.4, 5.5, 5.6, and 5.7.

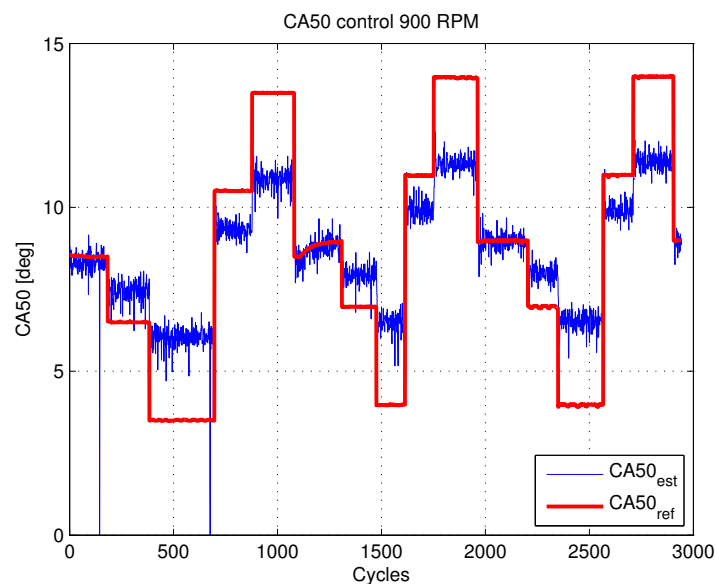


Figure 5.4: The control of CA50 at operating point 900 *RPM* with different values on the torque.

In Figure 5.4 the estimated and reference values of CA50 are displayed. The reference value of CA50 comes from the investigation of what value CA50 takes without control, at different operating points. In this case, the reference is shifted by ± 2 or ± 5 degrees to investigate how the controller handles a reference that is not optimal. It can be seen that the estimated CA50 follows the reference, but with a steady state error.

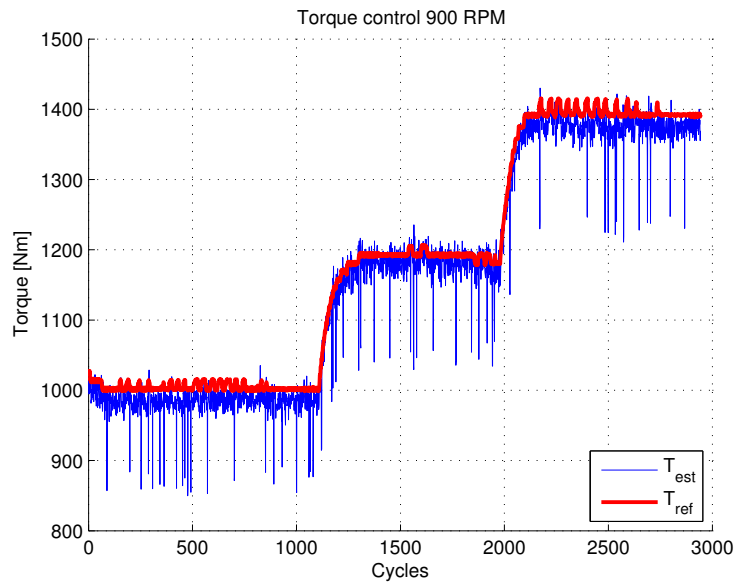


Figure 5.5: The control of the torque at operating point 900 *RPM* with different values on the torque.

Figure 5.5 illustrate the estimated and reference values of the torque. The reference value is the indicated torque. The illustration shows that the estimated torque follows the reference.

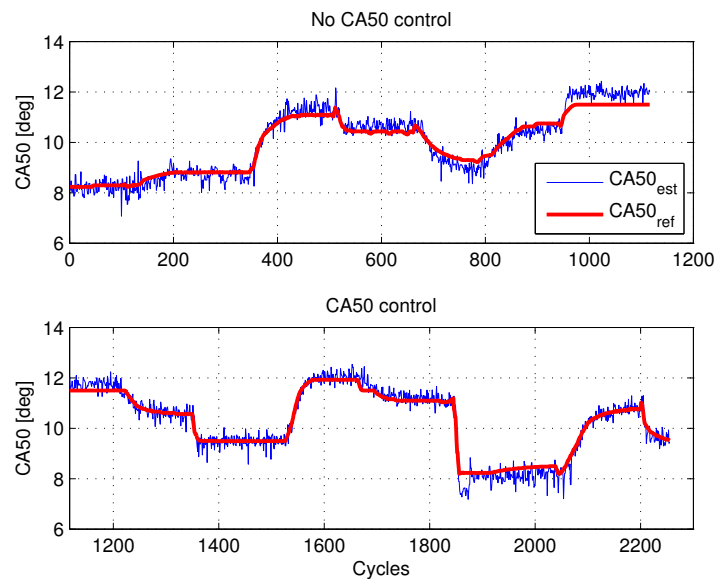


Figure 5.6: Estimated and reference signal of CA50 with and without control.

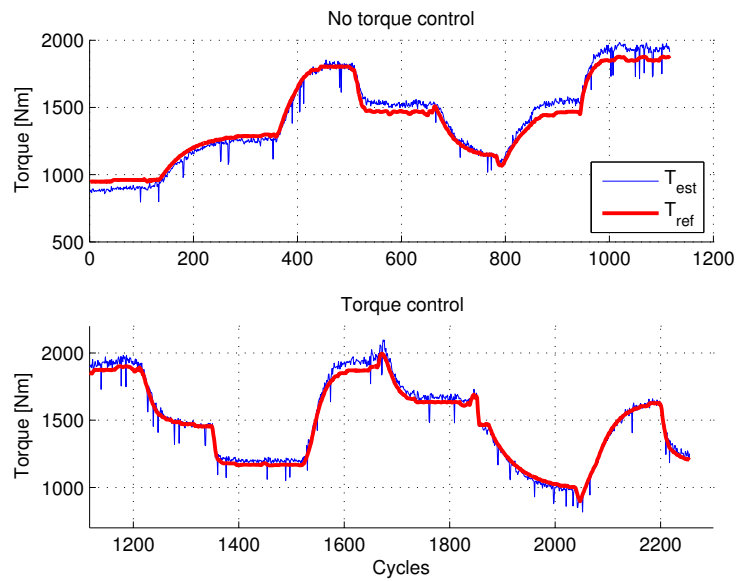


Figure 5.7: Estimated and reference signal of the torque with and without control.

In Figure 5.6 and 5.7 a comparison between how the estimate follows the reference signal, with and without control, at different operating points are illustrated. From these figures, it is clear that the estimates follow the references, both when the controller is on and off. However, when the controller is on, the performance is slightly improved.

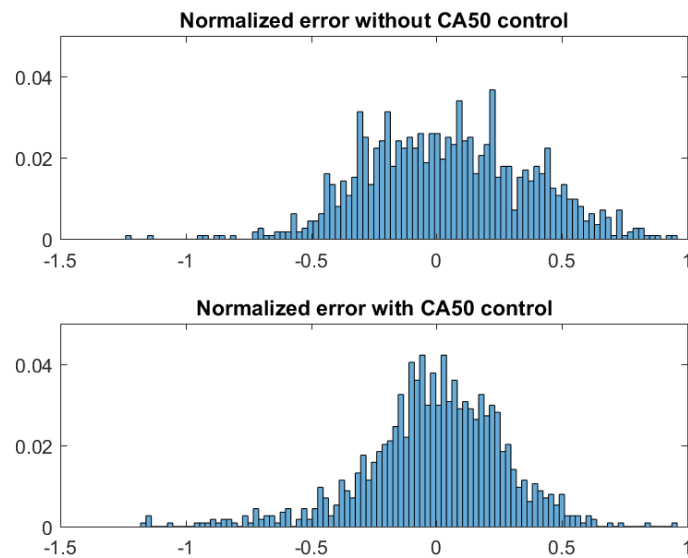


Figure 5.8: Histogram of the error for CA50, with and without control.

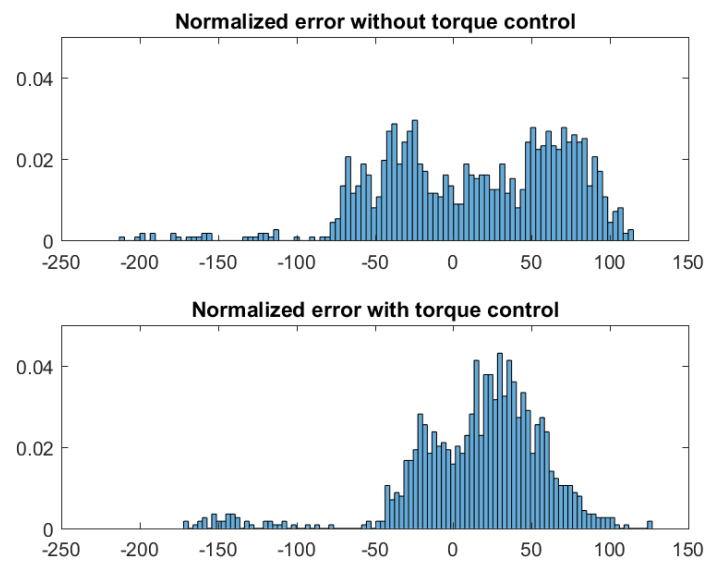


Figure 5.9: Histogram of the error for the torque, with and without control.

Figure 5.8 and 5.9 displays the normalized error between the reference and estimates for both CA50 and the torque. It can be seen that the distribution of the error is larger when the controller is off, indicating that the performance is, in fact, slightly improved when the controller is on.

6

Discussion

When developing both the estimates and the controller, several interesting results have been observed. The estimation of CA50 is successful in both simulations and engine tests. However, since there exists no exact reference it is hard to know how well the estimation works. Several simplifications and limitations contribute to less accurate results. The main simplification of the estimation of CA50 is that the convective heat transfer is not included in the model. This has the consequence that the total heat release will not reach the true maximum value. Since the slope is steep though, the estimation of CA50 will not be affected substantially.

Another aspect affecting the accuracy of the estimation is the sampling interval and the fact that samples are missing in engine tests. The interpolation of the pressure is linear and the effects of it can be seen in the heat release curve. To decrease the error given by the sampling interval, interpolation of CA50 is done, which especially decreases the error when the sampling interval is six degrees. This makes the estimates less sensitive to large sampling intervals.

Estimations of the exact TDC-offset was complex to calculate and in this project, the offset was found and compensated manually. This means that there might still exist a TDC-offset with the consequence that the pressure vector is shifted compared to the used θ -vector, which will introduce another possible error.

Another interesting result is that the estimate of CA50 is more noisy for lower torques. This has the consequence that the control of CA50 at low torques is harder to get correct. Since the possibility to test the controller was limited, the control was only tested on high torques.

When performing the engine tests on the controller, it could be seen that it worked well for small changes in the reference, but when the changes were larger a steady state offset occurs. To solve this, integral action could be included in the controller.

It could also be seen that the estimated CA50 follows the reference when the controller was on. This means that if the ECM gives the wrong timing of the main injection due to, for example, wear of injectors or different qualities of fuel, the controller may be able to compensate for this.

A similar result can be seen when controlling the torque. The difference compared to controlling CA50 is that the estimated torque manages to follow the reference

at rapid transients, without having a steady state error. The control of the torque contributes, in a similar way as the control of CA50, to give the correct amount of fuel to the engine, even if there are for example wear of injectors or for different quality of fuel.

If it was possible to control the heat release from the pilot injection, the right amount of fuel could be injected depending on the system. Since it is preferable with a small injection, an accurate estimation is essential. Due to the slow sampling interval, an estimation of the heat release was not possible, but a detection method was developed instead.

In the first pilot detection method, the results from simulation were promising, but since the measurements from the engine contained noise with a similar shape as the reference curve, detection was not reliable. If there was no noise, detection would be possible since the behavior would be the same as in simulation. One way to resolve this problem could perhaps be to filter the signal, but when this was tested also the pilot injection effect on the curve was filtered away. Another way to solve the problem could possibly be to narrow the the window when convoluting the curves, and only look when the pilot injection should be visible.

The second pilot detection method looked at what effect the pilot injection had on the pressure curve instead. Also, this method showed promising results in simulation and in engine tests the results were acceptable. It was found that the pilot detection method worked better at higher engine speeds, and it can detect a pilot injection as small as 2 mg/str . This could be an indication that the threshold should be dependent on the engine speed. If a proper threshold was found, an implementation of a controller could be done. Worth mentioning is that there is no way to actually know that a pilot injection has been made, only that it has been requested and that it has been interpreted as detected.

6.1 Future work

The estimation of both the torque and CA50 works well at high torques but needs to be improved for low torque values. To do this, an investigation has to be done to understand why the estimation works worse at low torques. Also, if further advanced calculations were considered, including for example TDC-offset and convective heat release, a more accurate estimation could be attained.

For the pilot detection, an analysis of the threshold value has to be further investigated. To develop the detection further, different threshold values could be implemented to be able to detect different fuel quantities. A way to do this is, for example, by implementing a higher threshold for detection of larger quantities and a lower threshold to detect smaller quantities. If this is implemented, the pilot detection could be included in the MIMO control structure.

To improve the controller, one idea could be to investigate another method to calculate the B-matrix, for example by using the least mean square method. Additional efforts also need to be put on tuning the weights in the controller. In addition, the method could be improved by investigating more operating points and add an engine speed- and torque dependence to get a more accurate model. Another aspect that needs to be examined and resolved is the steady state error on the CA50 control. A suggestion is to introduce integral action in the controller.

General improvements would be to have a sensor in all the cylinders, to get correct estimates for every cylinder. Some aspects are the same in every cylinder, such as fuel quality, but others differ, such as TDC-offset and wear parts. Also, if the sensor could sample faster without any loss of measurements, the estimates would be more accurate.

7

Conclusion

By utilizing measurements from in-cylinder pressure sensors, it is possible to estimate and control several important parameters with direct feedback. In this thesis, estimation of CA50 has been developed and two methods for pilot detection has been investigated. A MIMO control structure has been constructed and implemented in `TargetLink` for control of torque and CA50. All methods have been tested in simulations and in an engine test cell.

To estimate CA50, Heywood's formula for heat release calculations has been used. The result from both simulations and engine tests implies that the estimation is fairly correct, but sources of error are present. More advanced calculations could remove some of these and improve the result. The method works better at high torques but needs to be further developed to work with low torques as well.

The pilot detection was done through two alternative methods: pattern recognition and pressure difference. The first method convolutes a reference curve with the derivative of the heat release rate and uses a threshold to see if a pilot injection has occurred. This method showed promising results in simulations, but the measurements from the engine were too noisy to produce accurate results. The second method compares the measured pressure with a reference pressure curve, where no injections are done. This method also uses a threshold, since the pressure difference is larger when a pilot injection has occurred. Both simulations and engine tests generated promising results, and it was even possible to detect small quantities of pilot injection. The current threshold works better for higher engine speeds and should probably have an engine speed dependence.

The MIMO controller used is an LQ-controller. The state space model was developed through trial and error parameter identification and the tuning was done online. When analyzing the results, it could be seen that the estimates followed the references well during slow transitions. When the transitions were faster, the torque still managed to follow the reference, but a steady state error occurred in the control of CA50. This means that it is possible to compensate for worn engine parts and differences in fuel quality, among others.

Bibliography

- [1] R Ikemura, Y Yamasaki, and S Kaneko. Study on model based combustion control of diesel engine with multi fuel injection. In *Journal of Physics: Conference Series*, volume 744, page 012103. IOP Publishing, 2016.
- [2] John B Heywood et al. *Internal combustion engine fundamentals*, volume 930. Mcgraw-hill New York, 1988.
- [3] Kamran Eftekhari Shahroudi. *Robust design evolution and impact of in-cylinder pressure sensors to combustion control and optimization: A systems and strategy perspective*. PhD thesis, Massachusetts Institute of Technology, 2008.
- [4] Jason Hill, Erik Nelson, David Tilman, Stephen Polasky, and Douglas Tiffany. Environmental, economic, and energetic costs and benefits of biodiesel and ethanol biofuels. *Proceedings of the National Academy of sciences*, 103(30):11206–11210, 2006.
- [5] Dirk Schiefer, Ralf Maennel, and Wesley Nardoni. Advantages of diesel engine control using in-cylinder pressure information for closed loop control. Technical report, 2003.
- [6] Anton Kjellin and Per-Sebastian Pettersson. Torque estimation from in-cylinder pressure sensor for closed loop torque control. Master’s thesis, Institutionen för signaler och system, Chalmers tekniska högskola, 2017.
- [7] Mark C Sellnau, Frederic A Matekunas, Paul A Battiston, Chen-Fang Chang, and David R Lancaster. Cylinder-pressure-based engine control using pressure-ratio-management and low-cost non-intrusive cylinder pressure sensors. Technical report, SAE Technical paper, 2000.
- [8] Lino Guzzella and Christopher Onder. *Introduction to modeling and control of internal combustion engine systems*. Springer Science & Business Media, 2009.
- [9] X Luo, S Velayutham, and FPT Willems. Experimental validation of combustion control with multi-pulse fuel injection. 2017.
- [10] Hannu Jääskeläinen. Fuel injection for clean diesel engines. https://www.dieselnet.com/tech/engine_fi.php, 2017. [Online; accessed Januari 18 , 2018].

- [11] Tosaka. Diesel engine (4 cycle running), modified, 2009. [CC BY 3.0 (<http://creativecommons.org/licenses/by/3.0>)], via Wikimedia Commons, Online; accessed March 12, 2018.
- [12] Fabrizio Ponti, Vittorio Ravaglioli, Gabriele Serra, and Federico Stola. Instantaneous engine speed measurement and processing for mfb50 evaluation. *SAE International Journal of Engines*, 2(2):235–244, 2010.
- [13] Krzysztof Z Mendera, Andrzej Spyra, and Michał Smereka. Mass fraction burned analysis. *Journal of KONES Internal Combustion Engines*, 3:193–201, 2002.
- [14] Shreyas Dwarakanath and Viktor Eklind. Analysis of various heat release models for closed loop combustion control in a heavy duty diesel engine. *Volvo Trucks Summer Internship, internal investigation*, 2017.
- [15] Torkel Glad and Lennart Ljung. *Control theory*. CRC press, 2014.